The Journal of Chemical Physics

Implementation of symmetry-adapted perturbation theory based on density functional theory and using hybrid exchange-correlation kernels for dispersion terms

Cite as: J. Chem. Phys. **157**, 024801 (2022); https://doi.org/10.1063/5.0090688 Submitted: 08 March 2022 • Accepted: 10 June 2022 • Accepted Manuscript Online: 13 June 2022 • Published Online: 14 July 2022

Daniel G. A. Smith and C. C. David Sherrill







ARTICLES YOU MAY BE INTERESTED IN

Density-functional theory vs density-functional fits

The Journal of Chemical Physics 156, 214101 (2022); https://doi.org/10.1063/5.0091198

A consistent and accurate ab initio parametrization of density functional dispersion correction (DFT-D) for the 94 elements H-Pu

The Journal of Chemical Physics 132, 154104 (2010); https://doi.org/10.1063/1.3382344

Quantum Chemistry Common Driver and Databases (QCDB) and Quantum Chemistry Engine (QCEngine): Automation and interoperability among computational chemistry programs

The Journal of Chemical Physics 155, 204801 (2021); https://doi.org/10.1063/5.0059356



The Journal of Chemical Physics Special Topics Open for Submissions

Implementation of symmetry-adapted perturbation theory based on density functional theory and using hybrid exchange-correlation kernels for dispersion terms

Cite as: J. Chem. Phys. 157, 024801 (2022); doi: 10.1063/5.0090688 Submitted: 8 March 2022 • Accepted: 10 June 2022 •









Published Online: 14 July 2022



Yi Xie, Daniel G. A. Smith, Daniel G. A. Smith, David Sherrill Daniel G. A. Smith, Daniel G. David Sherrill



AFFILIATIONS

Center for Computational Molecular Science and Technology, School of Chemistry and Biochemistry, School of Computational Science and Engineering, Georgia Institute of Technology, Atlanta, Georgia 30332-0400, USA

- Present address: Entos, Inc. 4470 W. Sunset Blvd., Suite 107 PMB 94758, Los Angeles, CA 90027, USA.
- b) Author to whom correspondence should be addressed: sherrill@gatech.edu

ABSTRACT

We report the implementation of a symmetry-adapted perturbation theory algorithm based on a density functional theory [SAPT(DFT)] description of monomers. The implementation adopts a density-fitting treatment of hybrid exchange-correlation kernels to enable the description of monomers with hybrid functionals, as in the algorithm by Bukowski, Podeszwa, and Szalewicz [Chem. Phys. Lett. 414, 111 (2005)]. We have improved the algorithm by increasing numerical stability with QR factorization and optimized the computation of the exchange-correlation kernel with its 2-index density-fitted representation. The algorithm scales as $O(N^5)$ formally and is usable for systems with up to ~3000 basis functions, as demonstrated for the C₆₀-buckycatcher complex with the aug-cc-pVDZ basis set. The hybrid-kernelbased SAPT(DFT) algorithm is shown to be as accurate as SAPT(DFT) implementations based on local effective exact exchange potentials obtained from the local Hartree-Fock (LHF) method while avoiding the lower-scaling $[O(N^4)]$ but iterative and sometimes hard-to-converge LHF process. The hybrid-kernel algorithm outperforms Hartree-Fock-based SAPT (SAPT0) for the S66 test set, and its accuracy is comparable to the many-body perturbation theory based SAPT2+ approach, which scales as $O(N^7)$, although SAPT2+ exhibits a more narrow distribution of errors.

Published under an exclusive license by AIP Publishing. https://doi.org/10.1063/5.0090688

I. INTRODUCTION

Symmetry Adapted Perturbation Theory (SAPT)¹⁻³ is known as one of the most powerful methods for studying intermolecular interactions. A key advantage of SAPT is its clear physical interpretation; each term in SAPT can be attributed to a certain type of intermolecular force. This provides additional physical insight, especially when investigating systems with more complex interactions, such as π - π interactions, which feature important contributions from both electrostatics and London dispersion interactions.⁴ Perhaps the most commonly used variant of SAPT, SAPT0, uses a Hartree–Fock description of monomers, and the interaction between monomers is modeled as a perturbation to the non-interacting system. While being computationally inexpensive compared to many quantum

mechanical models, SAPT0 completely neglects the electron correlation within each monomer, which could lead to inaccurate component energies and total interaction energies. The conventional many-body SAPT methods address this shortcoming by employing a triple-perturbation theory with the intermolecular interaction and intramolecular fluctuation potentials as different perturbations. Unfortunately, this approach is computationally costly, with the formal scaling of $O(N^6)$ and higher, and would not be affordable for larger systems, particularly many systems of biological

Alternatively, a mixture of density functional theory (DFT) and SAPT has been developed, known as SAPT(DFT) or DFT-SAPT by different groups of developers. The original idea of SAPT(DFT) was proposed in 2001 by Williams and Chabalowski⁵ by replacing the Hartree-Fock description of monomers with Kohn-Sham DFT, expecting that the effect of the exchange-correlation (xc) potential in DFT would go into the Kohn-Sham orbitals and that these modified orbitals would allow some approximate accounting of intramolecular correlation effects in the SAPT terms. This scheme was extremely appealing in that the intramolecular correlation could be included in SAPT with a drastic reduction in computational time, compared to the conventional many-body SAPT method. However, while this approach correctly predicted binding for many typical dimer systems (as opposed to supermolecular HF and DFT), it failed to outperform SAPT0 quantitatively, especially in second-order terms. Williams and Chabalowski attributed the failure for second-order terms to the underestimation of the occupied-virtual orbital energy gap in most contemporary DFT functionals.6 They also noticed the trend that the first-order energies were more likely to fail for large intermolecular distances and nonpolar systems, but the main cause of this problem was not immediately apparent.

Based on these drawbacks of the original SAPT(DFT) scheme, later referred to as SAPT(KS) after SAPT(DFT) was further developed into a more sophisticated theory, Jansen and Hesselmann published an insightful comment pointing out two crucial facts. First, the SAPT(KS) method is not potentially exact, i.e., it would not be exact even if the exact exchange-correlation potential was available for all terms except for $E_{\rm elst}^{(1)}$. This is because the zeroth-order wavefunction in SAPT(KS) is the so-called Kohn–Sham wavefunction under the Kohn-Sham DFT framework. The Kohn-Sham system would generate the same density as the electronic system and thus the correct electrostatic energy, which solely depends on the electronic density. However, $E_{\rm exch}^{(1)}$ depends on density matrices, and the Kohn-Sham wavefunction is not guaranteed to describe the density matrices of the system correctly, and therefore, $E_{\rm exch}^{(1)}$ is not potentially exact. Likewise, this also applies to other higher order terms that have dependencies on density matrices. Furthermore, the second-order energies in SAPT(KS) were calculated using sum-over-state formulas, which corresponds to using what is referred to in SAPT as an "uncoupled" approximation that neglects orbital relaxation effects, i.e., the changes in Coulomb and exchange-correlation potentials in response to the perturbation-induced change in the electron density. In SAPT0 and other higher-order HF-based SAPT theories, "coupled" induction terms have generally been used, 1,8 and Patkowski et al. justified this by writing induction energy as the minimum of a functional of the orbitals.9

It is worth pointing out that although $E_{\rm elst}^{(1)}$ is potentially exact, the quantitative accuracy of it was not satisfactory in the original work of Williams and Chabalowski,⁵ and they conjectured that the poor accuracy could be due to the poor description of electronic density of DFT in the asymptotic area. This conjecture was confirmed by Hesselmann and Jansen (HJ),¹⁰ and they applied an asymptotic correction to the PBE0 functional of Perdew *et al.*^{11,12} by splicing it with the asymptotically correct LB94 functional of van Leeuwen and Baerends¹³ through the gradient-regulation asymptotic correction (GRAC) scheme.¹⁴ The use of PBE0 together with LB94 and the GRAC scheme is referred to as PBE0AC by HJ. Misquitta and Szalewicz (MS) independently confirmed the above conjecture,¹⁵ and they proposed to use the Fermi–Amaldi¹⁶ function in the asymptotic range, together with the splicing scheme

of Tozer and Handy. 17 Both asymptotic correction schemes correct the wrong asymptotic behavior of the GGA functionals, which decay exponentially, while the exact xc-potential should decay as 1/r. This allowed the accurate reproduction of electron density in a long range¹⁸ and thus produced more accurate first-order and induction energies. 8,10,15 To include the orbital relaxation effects, HJ and MS independently reformulated the equations for induction^{8,13} and dispersion^{20,21} energies in terms of frequency-dependent density-density response functions or frequency-dependent density susceptibilities (FDDS). MS and co-workers also pointed out that the "uncoupled" sum-over-state formulas for induction and dispersion energies are equivalent to using the Kohn-Sham wavefunction as an approximation to the exact electronic wavefunction, 21 i.e., the uncoupled FDDS is equivalent to that of the Kohn-Sham system, and the coupled FDDS is equivalent to that of the true electronic system. With the coupled FDDS that is available from coupledperturbed time-dependent density functional theory (TDDFT), the induction and dispersion energies could be potentially exact. On the other hand, HJ have shown that for SAPT(DFT), the correct long-range behavior (and thus physically correct virtual orbital eigenvalues from an asymptotically corrected xc-potential) is not sufficient for computing the dispersion energy accurately without using the coupled FDDS, i.e., the virtual orbital eigenvalue issue is not the only reason for the failure of SAPT(KS) in second-order terms.

In the above SAPT(DFT) scheme, the most expensive part would be solving for the coupled FDDS from the TDDFT equations and computing the dispersion energy from the coupled FDDS, both of which scale as $O(N_{occ}^3N_{vir}^3)$, where N_{occ} and N_{vir} represent the number of occupied and virtual orbitals, respectively. The density-fitting technique^{22,23} has been used by both groups developing SAPT(DFT). In both approaches, the adiabatic local-density approximation (ALDA) of the xc kernel has been employed, and it has been shown that such an approximation is satisfactory for computing response properties and dispersion energies, ^{21,24} but a hybrid ALDA kernel (i.e., linear combination of HF and ALDA kernels) would be required for hybrid xc-potentials in order to reproduce accurate dispersion energies. ^{20,25}

With the density-fitting technique, the scaling of solving the TDDFT equation with the pure ALDA kernel for FDDS is $O(N_{occ}N_{vir}N_{aux}^2)$, ²⁵ and computing the dispersion energy from the FDDS scales as $O(N_{aux}^3)$, where N_{aux} is the number of densityfitting auxiliary functions. Bukowski et al. developed an approach to compute the coupled FDDS with the hybrid ALDA kernel using the density-fitting approximation.²⁷ This algorithm has to handle the Hartree-Fock-like exchange terms in the hybrid ALDA kernel and thus scales as $O(N_{occ}^2 N_{vir}^2 N_{aux}^2)$. On the other hand, Hesselmann and Jansen developed a scheme²⁵ replacing the Hartree-Fock-like exchange part in the xc-potential by a local effective exact exchange potential, which is obtained using the local Hartree-Fock (LHF) method by Della Sala and Görling.²⁸ They have also shown in the same work that combining this localized xc-potential, named LPBEOAC, and the pure ALDA kernel generates nearly identical dispersion energies as the non-localized PBE0AC potential combined with a hybrid ALDA kernel. Both approaches have enabled the use of a hybrid functional in SAPT(DFT), with one nominally scaling as $O(N^5)$ and another as $O(N^4)$, but the latter has a

larger prefactor due to the self-consistent LHF calculation. It is also worth pointing out that even if the LHF approach has an $O(N^4)$ scaling for the coupled dispersion term with density-fitting, the exchange-dispersion term, whether uncoupled or coupled, would not benefit significantly from density-fitting and still scales as $O(N^5)$ nominally.

One main restriction in applying SAPT(DFT) to larger systems is the need to generate intermediate tensors that are too large to store in main memory, so they must be stored on disk. In the SAPT2020 code developed by Szalewicz and co-workers, 29 the disk space requirement is $O(N^4)$ for hybrid functionals, which should limit the size of the system to roughly 1000 basis functions, although the user has the choice to use non-hybrid functionals to avoid this limitation. Another major improvement on the SAPT(DFT) dispersion algorithm was the use of a 2-index representation $(P|f_{xc}|Q)$ for the xc kernel by Pitoňák and Hesselmann, 30 instead of the 3-index representation $(ia|f_{xc}|P)$ used in earlier work. 25,27 In addition to the 2-index representation, Pitoňák and Hesselmann also introduced a grid-free algorithm 30 identical to grid-free DFT methods of Almlöf and co-workers, $^{31-33}$ reducing the cost computing $(P|f_{xc}|Q)$ significantly by avoiding computations on a grid, which typically has a size of 10^5-10^6 for larger systems.

In this work, we introduce and implement an algorithm for SAPT(DFT) based on the algorithms by Jansen and Szalewicz, with substantial improvements for the dispersion terms. Our algorithm is capable of computations with hybrid functionals without the use of LHF approximations while reducing the disk requirement to $O(N^3)$ by careful handling of 4-index integrals and 4-index tensors, allowing the code to work for larger systems with up to 3000 basis functions. We have also integrated Pitonak and Hesselmann's 2-index xc kernel representation³⁰ into our code with support for hybrid ALDA kernels. In addition, while Ref. 34 suggested an effective method for estimating coupled exchange-dispersion energies by scaling the uncoupled energies by a fixed factor, we noticed that the factor would be accurate only for uncoupled exchangedispersion energies computed from Kohn-Sham orbitals with the LHF approximation; therefore, we have also estimated and tested a new scaling factor for non-LHF orbitals using the S22 \times 5 and $S66 \times 8 \text{ datasets.}^3$

In this work, we report details of our implementation and the aforementioned new scaling factor to estimate coupled exchange-dispersion energies from uncoupled ones, test the accuracy of the interaction energies and their components, and examine the computational efficiency of the code. Our SAPT(DFT) code is publicly available as part of the open-source PSI4 quantum chemistry program package.³⁹

II. THEORY

A. JK-based terms

In our SAPT(DFT) code, the first-order (electrostatics and exchange) and induction terms can be computed from the molecular orbital (MO) coefficients and generalized coulomb and exchange (J and K) matrices, in addition to the coupled-perturbed Kohn–Sham (CPKS) amplitudes for coupled induction energies. As opposed to the usual JK matrices that are functionals of the density matrix, generalized JK matrices are the functions of arbitrary

matrices **D** of size $N_{AO} \times N_{AO}$, where N_{AO} is the number of atomic orbitals,

$$(\mathbf{J}[\mathbf{D}])_{\mu\nu} = \sum_{\lambda\sigma} \mathbf{D}_{\lambda\sigma}(\mu\nu|\lambda\sigma),\tag{1}$$

$$(\mathbf{K}[\mathbf{D}])_{\mu\nu} = \sum_{\lambda\sigma} \mathbf{D}_{\lambda\sigma}(\mu\lambda|\nu\sigma). \tag{2}$$

Details are given in Refs. 1 and 40. Here, we follow the equations of Ref. 25 for electrostatics, exchange, and induction terms. We do not repeat the derivation of these equations here, but we refer the reader to Refs. 1, 25, and 40 for more details on the origins of the working equations for these JK-based terms. We will be using the element-wise dot products in the following equations. The dot product between square matrices **A** and **B** is defined as

$$\mathbf{A} \cdot \mathbf{B} = \sum_{i,j} A_{ij} B_{ij} = \mathrm{Tr}(\mathbf{AB}). \tag{3}$$

The electrostatic energy is given by

$$E_{\text{olet}}^{(1)} = 2\mathbf{P}^A \cdot \mathbf{V}^B + 2\mathbf{P}^B \cdot \mathbf{V}^A + 4\mathbf{P}^B \cdot \mathbf{J}^A + V_{\text{nuc}}, \tag{4}$$

where $\mathbf{P}^{\mathbf{X}}(X = \text{monomers } A \text{ and } B)$ is the one-particle density matrix, constructed from the occupied-orbital columns of each isolated-monomer SCF coefficient matrix,

$$\mathbf{P}^{X} = \mathbf{C}^{X,occ} (\mathbf{C}^{X,occ})^{\dagger}, \tag{5}$$

where \mathbf{V}^X is the nuclear potential, \mathbf{J}^X is the Coulomb matrix, and V_{nuc} is the (intermolecular) nuclear repulsion energy. The first two terms of Eq. (4) provide electron-nuclear attraction, and the third term provides electron–electron repulsion ($\mathbf{P}^A \cdot \mathbf{J}^B = \mathbf{P}^B \cdot \mathbf{J}^A$, so we have combined these terms).

The exchange energy in the S^2 approximation (i.e., linear approximation in terms of permutation operator in the antisymmetrizer) is given by

$$E_{\text{exch}}^{(1)}(S^{2}) = -2(\mathbf{P}^{A}\mathbf{S}^{AO}\mathbf{P}^{B}\mathbf{S}^{AO}\mathbf{P}^{A,vir}) \cdot \boldsymbol{\omega}^{B}$$
$$-2(\mathbf{P}^{B}\mathbf{S}^{AO}\mathbf{P}^{A}\mathbf{S}^{AO}\mathbf{P}^{B,vir}) \cdot \boldsymbol{\omega}^{A}$$
$$-2(\mathbf{P}^{A,vir}\mathbf{S}^{AO}\mathbf{P}^{B}) \cdot \mathbf{K}[\mathbf{P}^{A}\mathbf{S}^{AO}\mathbf{P}^{B,vir}], \tag{6}$$

where $\mathbf{P}^{X,vir}$ is a density-like matrix but constructed from the virtual-orbital columns of the SCF coefficient matrices,

$$\mathbf{P}^{X,vir} = \mathbf{C}^{X,vir} (\mathbf{C}^{X,vir})^{\dagger}, \tag{7}$$

 ω^{X} represents the electrostatic potential generated by the electrons and nuclei of monomer X,

$$\boldsymbol{\omega}^X = 2\mathbf{J}^X + \mathbf{V}^X,\tag{8}$$

and \mathbf{S}^{AO} is the overlap matrix under the atomic orbital basis.

The full S^{∞} exchange energy (without the S^2 approximation) is given by

$$E_{\text{exch}}^{(1)} = -2\mathbf{P}^{A} \cdot \mathbf{K}^{B} + 2\mathbf{T}^{AB} \cdot \left(\mathbf{h}^{A} + \mathbf{h}^{B}\right) + 2\mathbf{T}^{AA} \cdot \mathbf{h}^{B} + 2\mathbf{T}^{BB} \cdot \mathbf{h}^{A}$$

$$+ 2\mathbf{T}^{BB} \cdot \mathbf{W}^{AB} + 2\mathbf{T}^{AA} \cdot \mathbf{W}^{AB} + 2\mathbf{T}^{BB} \cdot \mathbf{W}^{AA} + 2\mathbf{T}^{AB} \cdot \mathbf{W}^{AB},$$
(9)

where

$$\mathbf{h}^X = \mathbf{V}^X + 2\mathbf{J}^X - \mathbf{K}^X,\tag{10}$$

$$\mathbf{T}^{XY} = \mathbf{C}^{X,occ} \mathbf{T}_{MO}^{XY} (\mathbf{C}^{Y,occ})^{\dagger}, \tag{11}$$

$$\mathbf{W}^{XY} = 2\mathbf{J} [\mathbf{T}^{XY}] - \mathbf{K} [\mathbf{T}^{XY}], \tag{12}$$

$$\mathbf{T} = \begin{bmatrix} \mathbf{1} & \mathbf{S}^{MO} \\ (\mathbf{S}^{MO})^{\mathsf{T}} & \mathbf{1} \end{bmatrix}^{-1} - \begin{bmatrix} \mathbf{1} & \mathbf{0} \\ \mathbf{0} & \mathbf{1} \end{bmatrix}, \tag{13}$$

where \mathbf{T}_{MO}^{XY} is the block of \mathbf{T} corresponding to molecular orbitals of X in rows and Y in columns and \mathbf{S}^{MO} is the overlap matrix under the molecular orbital basis.

The induction energy, which consists of the interaction arising from the perturbation of monomer A by the (unperturbed) static electric field of monomer B ($E_{\text{ind}}^{(2)}(A \leftarrow B)$), and vice versa ($E_{\text{ind}}^{(2)}(A \rightarrow B)$), is given by

$$E_{\text{ind}}^{(2)}(A \leftarrow B) = 2\mathbf{x}^A \cdot \tilde{\boldsymbol{\omega}}^B, \tag{14}$$

$$E_{\text{ind}}^{(2)}(A \to B) = 2\mathbf{x}^B \cdot \tilde{\boldsymbol{\omega}}^A, \tag{15}$$

where \mathbf{x}^X represents the response of monomer X to the electric potential of the other monomer, solved for using coupled-perturbed Kohn–Sham as described below, and expressed in the basis of occupied and virtual molecular orbitals of monomer X. $\tilde{\boldsymbol{\omega}}^X$ is the electric potential of monomer X [Eq. (8), originally expressed in the atomic orbital basis] transformed into the occupied-virtual MO product space of monomer Y so that it can be dotted against \mathbf{x}^Y in the above expressions for the induction energy,

$$\tilde{\boldsymbol{\omega}}^{X} = (\mathbf{C}^{Y,occ})^{\dagger} \boldsymbol{\omega}^{X} \mathbf{C}^{Y,vir}. \tag{16}$$

The exchange-induction term under the S^2 approximation is

$$E_{\text{exch-ind}}^{(2)}(S^2)(A \leftarrow B) = 2\mathbf{x}^A \cdot \left((\mathbf{C}^{A,occ})^{\dagger} (-\mathbf{K}^B - 2\mathbf{J}[\mathbf{O}] + \mathbf{K}[\mathbf{O}] + 2\mathbf{J}[\mathbf{P}^B \mathbf{S}^{AO} \mathbf{O}] + \mathbf{S}^{AO} \mathbf{P}^B \right) \times \left(-\mathbf{h}^A + \mathbf{S}^{AO} \mathbf{P}^A \boldsymbol{\omega}^B + \boldsymbol{\omega}^A \mathbf{P}^B \mathbf{S}^{AO} - \mathbf{K}[\mathbf{O}]^T \right) + \left(-\mathbf{h}^B + \boldsymbol{\omega}^B \mathbf{P}^A \mathbf{S}^{AO} - \mathbf{K}[\mathbf{O}]^T \right) + (\mathbf{D}^B \mathbf{S}^{AO}) \mathbf{C}^{A,vir},$$

$$(17)$$

$$E_{\text{exch-ind}}^{(2)}(S^{2})(A \to B) = 2\mathbf{x}^{B} \cdot \left((\mathbf{C}^{B,occ})^{\dagger} \left(-\mathbf{K}^{A} - 2\mathbf{J}[\mathbf{O}] \right) \right.$$

$$+ \mathbf{K}[\mathbf{O}] + 2\mathbf{J}[\mathbf{P}^{A}\mathbf{S}^{AO}\mathbf{O}] + \mathbf{S}^{AO}\mathbf{P}^{A}$$

$$\times \left(-\mathbf{h}^{B} + \mathbf{S}^{AO}\mathbf{P}^{B}\boldsymbol{\omega}^{A} + \boldsymbol{\omega}^{B}\mathbf{P}^{A}\mathbf{S}^{AO} \right.$$

$$- \mathbf{K}[\mathbf{O}]^{T} \right) + \left(-\mathbf{h}^{A} + \boldsymbol{\omega}^{A}\mathbf{P}^{B}\mathbf{S}^{AO} \right.$$

$$- \mathbf{K}[\mathbf{O}](\mathbf{P}^{A}\mathbf{S}^{AO})\mathbf{C}^{B,vir} \right), \tag{18}$$

where

$$\mathbf{O} = \mathbf{P}^A \mathbf{S}^{AO} \mathbf{P}^B. \tag{19}$$

For uncoupled induction and exchange-induction energies, the amplitudes are

$$\left(\mathbf{x}^{X}\right)_{r}^{a} = -\frac{\left(\tilde{\boldsymbol{\omega}}^{Y}\right)_{r}^{a}}{\epsilon_{r} - \epsilon_{a}},\tag{20}$$

where a and r run over all occupied and virtual molecular orbitals, respectively, of monomer X.

For coupled induction, the amplitudes are solved from the CPKS equations, where \mathbf{x} and $\boldsymbol{\omega}$ are treated as $(N_{occ}N_{vir})$ -dimensional vectors. The CPKS equations can be expressed as the following linear system of equations:

$$\mathbf{H}^{(1)}\mathbf{x}^A = \boldsymbol{\omega}^B,\tag{21}$$

$$\mathbf{H}^{(1)}\mathbf{x}^B = \boldsymbol{\omega}^A,\tag{22}$$

and the CPKS Hessian $\mathbf{H}^{(1)}$ can be constructed from

$$\mathbf{H}^{(1)} = \mathbf{d} + 4\mathbf{H}_0^{(1)} + \mathbf{H}_r^{(1)}, \tag{23}$$

$$(\mathbf{d})_{ar\,a'r'} = (\epsilon_r - \epsilon_a)\delta_{aa'}\delta_{rr'},\tag{24}$$

$$\left(\mathbf{H}_{0}^{(1)}\right)_{ar,a'r'} = \left(ar|a'r'\right) + \int \phi_{a}\phi_{r}\phi_{a'}\phi_{r'}\frac{\delta v_{xc}}{\delta\rho}d\mathbf{r}, \tag{25}$$

$$\left(\mathbf{H}_{r}^{(1)}\right)_{ar\,a'r'} = -\xi \left[\left(aa'|rr'\right) + \left(ar'|a'r\right)\right]. \tag{26}$$

The CPKS equations can be solved using the conjugate gradient solver in PS14 designed for CPHF, with a slight modification by adding a v_{xc} matrix to the **J** matrix and scaling **K** by ξ , where v_{xc} is the exchange–correlation potential and ξ is the fraction of Hartree–Fock exchange in the DFT xc potential.

B. Asymptotic correction

As introduced before, HJ performed asymptotic correction on PBE0 by splicing it with LB94 using the gradient-regulated asymptotic correction (GRAC) scheme reported by Grüning *et al.*¹⁴ Another common correction scheme, the Fermi–Amaldi–Tozer–Handy correction, mainly adopted by MS and co-workers is not yet implemented in PS14.

In the framework of GRAC, the general form of the asymptotically corrected xc potential can be written as a linear combination of the bulk region potential v_{xc}^b and the asymptotic correction potential

$$v_{xc}^{b-AC}(\mathbf{r}) = [1 - f(\mathbf{r})]v_{xc}^b(\mathbf{r}) + f(\mathbf{r})v_{xc}^a(\mathbf{r}).$$
 (27)

In the instance of PBE0AC, v_{xc}^b is PBE0, which is the base functional, and v_{xc}^{a} is LB94, a functional that is asymptotically correct but behaves poorly in the bulk region. In the GRAC scheme, the switching function $f(\mathbf{r})$ takes the following form:

$$f[x(\mathbf{r})] = \frac{1}{1 + e^{-\alpha[x(\mathbf{r}) - \beta]}},$$
(28)

$$x(\mathbf{r}) = \frac{|\nabla \rho(\mathbf{r})|}{\rho^{4/3}(\mathbf{r})}.$$
 (29)

With the form given, the switching function $f(\mathbf{r})$ approaches to unity in the asymptotic region and vanishes in the bulk region. As a result, the combined functional behaves similarly to PBE0 at short intermolecular distances r and to LB94 at large r, thus being able to combine the advantages of both functionals and reproduce accurate electron densities over all distances. One example can be found in Fig. 2 of Ref. 18, where the radial density of the neon atom is computed with HF, PBE0, LB94, and PBE0AC and compared with coupled-cluster single, double, and perturbative triple [CCSD(T)]⁴¹ densities as a benchmark.

As a consequence of the discontinuity of the exact xc potential as the number of electrons increases, 43 the exact potential should not vanish asymptotically but converge to, according to the generalized Koopmans' theorem, 1

$$v_{\text{XC},\sigma}(\infty) = \epsilon_{\text{HOMO},\sigma} + I_{\sigma},$$
 (30)

where $\epsilon_{\text{HOMO},\sigma}$ is the highest occupied Kohn-Sham orbital eigenvalue and I_{σ} is the ionization potential for removing the highest occupied electron of spin σ . Therefore, the value $v_{XC,\sigma}(\infty)$, also known as the asymptotic shift, becomes an essential parameter for the GRAC scheme to determine the proper asymptotic behavior of the corrected potential. In practice, $\epsilon_{\mathrm{HOMO},\sigma}$ is easily obtained from a conventional KS-DFT calculation (without the asymptotic shift), and the ionization potential is obtained either experimentally or computationally by explicitly computing the energy of the ionized state (e.g., M⁺ cation for a neutral molecule M).

C. Dispersion terms

In the traditional SAPT theory, the second-order dispersion term is written in a sum-over-state form, as introduced before,

$$E_{disp}^{(2)} = -4 \sum_{abrs} \frac{|(ar|bs)|^2}{\epsilon_{ar} + \epsilon_{bs}}.$$
 (31)

As mentioned before, the sum-over-state expression of the dispersion term corresponds to the uncoupled approximation of the dispersion energy of the system. With the Casimir-Polder identity, the dispersion term can be rewritten in terms of the uncoupled FDDS 44,45 as follows:

$$E_{disp}^{(2)} = -\frac{1}{2\pi} \int_0^{\infty} d\omega \int d\mathbf{r}_A d\mathbf{r}'_A d\mathbf{r}_B d\mathbf{r}'_B \frac{1}{|\mathbf{r}_A - \mathbf{r}_B|} \frac{1}{|\mathbf{r}'_A - \mathbf{r}'_B|} \times \chi_0^A (\mathbf{r}_A, \mathbf{r}'_A|i\omega) \chi_0^B (\mathbf{r}_B, \mathbf{r}'_B|i\omega), \tag{32}$$

$$\chi_0(\mathbf{r}, \mathbf{r}'|i\omega) = 4\sum_{ar} \frac{\epsilon_{ar}}{\epsilon_{ar}^2 + \omega^2} \phi_i(\mathbf{r}) \phi_a(\mathbf{r}) \phi_i(\mathbf{r}') \phi_a(\mathbf{r}'). \tag{33}$$

In Eq. (33), the FDDS is represented in the position space, and this gives it a clear physical interpretation: the linear response of density at the coordinate \mathbf{r}' with respect to a perturbation of density at the coordinate \mathbf{r} at the frequency $i\omega$ in the frequency domain. As mentioned above, the uncoupled FDDS $\chi_0(\mathbf{r},\mathbf{r}'|\omega)$ describes the linear response property of the Kohn–Sham wavefunction, and Eq. (32) would also give the dispersion energy of the Kohn-Sham system.²¹ The results in Ref. 20 show that such an approximation would result in an overestimation of dispersion energies by more than 30% on average. To compute the coupled dispersion energy, one would need to solve for the coupled FDDS from the TDDFT equation. In the response function formalism, the equation is written as

$$\chi(\mathbf{r}, \mathbf{r}'|\omega) = \chi_0(\mathbf{r}, \mathbf{r}'|\omega) + \int d\omega d\mathbf{r}_1 d\mathbf{r}_2 \chi_0(\mathbf{r}, \mathbf{r}_1|\omega)$$

$$\times \left[\frac{1}{r_{12}} + f_{xc}(\mathbf{r}_1, \mathbf{r}_2, \omega) \right] \chi(\mathbf{r}_2, \mathbf{r}'|\omega). \tag{34}$$

With the density fitting technique, the FDDS can be expressed in the auxiliary basis set representation with matrix elements $(P|\chi|Q)$. For non-hybrid xc potential and kernel, the solution of the coupled FDDS with the matrix representation is

$$\chi = \chi_0 + \chi_0 S^{-1} W (S - \chi_0 S^{-1} W)^{-1} \chi_0,$$
 (35)

where S is the Coulomb metric in the auxiliary basis set

$$\mathbf{S}_{PQ} = \left(P \left| \frac{1}{r_{12}} \right| Q \right), \tag{36}$$

and the operator W denotes the interelectronic interactions, including Coulomb, exchange, and correlation effects,

$$\mathbf{W}_{PQ} = \left(P \left| \frac{1}{r_{12}} \right| Q\right) + \left(P \left| f_{xc} \right| Q\right). \tag{37}$$

The xc kernel can be computed with a grid-free DFT algorithm proposed by Almlöf and co-workers, 30-33 where the xc kernel functional is imposed on the electron density operator $(P|\rho|Q)$ diagonalized in the DF auxiliary basis representation.

The dispersion energy may be computed by integrating over the FDDS,

$$E_{disp}^{(2)} = -\frac{1}{2\pi} \int_0^{\infty} d\omega (\mathbf{S}^{-1} \boldsymbol{\chi}^A \mathbf{S}^{-1}) \boldsymbol{\chi}^B.$$
 (38)

For a hybrid xc kernel, we have derived a set of equations based on the algorithm by Bukowski and co-workers in 2005.²⁷ Without the density fitting approximation, the FDDS [expressed in the orbital representation $\mathbf{C}_{ar,a'r'}(i\omega)$] can be solved from the following matrix equation from coupled Kohn–Sham theory:

$$\left(\mathbf{H}^{(2)}\mathbf{H}^{(1)} + \omega^2 \mathbf{I}\right) \mathbf{C}(i\omega) = -4\mathbf{H}^{(2)},\tag{39}$$

where I denotes the unit matrix of dimension $N_{occ}N_{vir}$, $\mathbf{H}^{(1)}$ is defined by Eq. (23), and $\mathbf{H}^{(2)}$ is written as follows:

$$\mathbf{H}^{(2)} = \mathbf{d} + \mathbf{H}_r^{(2)},$$
 (40)

$$\left(\mathbf{H}_{r}^{(2)}\right)_{ar.a'r'} = -\xi \left[\left(aa'|rr'\right) - \left(ar'|a'r\right)\right],\tag{41}$$

and \mathbf{d} is given in Eq. (24).

In the work of Bukowski $et\ al.,^{27}$ they proposed an algorithm to solve the above equation utilizing the density fitting technique. The algorithm lowers the $O(N^6)$ scaling of the non-DF version to $O(N^5)$, but it has several downsides: first, their algorithm is iterative, and we later discovered that this would not be necessary. Second, the xc kernel is represented as a 3-index tensor in this algorithm, and the evaluation of the kernel is also not as cheap as the grid-free DFT algorithm mentioned above. After utilizing the grid-free DFT algorithm and the 2-index DF auxiliary basis representation of the xc kernel and FDDS, along with the proper arrangement of the procedures of storing 3-index intermediates on the disk, we rewrite the results of Bukowski $et\ al.$ into the following form, which is a modification of Eq. (35):

$$\chi = \chi'_0 + (\chi'_0 \mathbf{S}^{-1} \mathbf{W} + \mathbf{K} (\mathbf{R}^T)^{-1} \mathbf{S}) [\mathbf{S} - (\chi'_0 \mathbf{S}^{-1} \mathbf{W} + \mathbf{K} (\mathbf{R}^T)^{-1} \mathbf{S})]^{-1} \chi'_0.$$
(42)

All quantities here are expressed in the density fitting auxiliary basis and have dimension $N_{aux} \times N_{aux}$. The matrix **K** includes the effect of Hartree–Fock type exchange integrals in the TDDFT Hessian,

$$\mathbf{K} = -\xi \left[\mathbf{K}_1(\lambda d) + \mathbf{K}_2(\lambda d) \right] + \xi^2 \mathbf{K}_{21}(\lambda), \tag{43}$$

which K can be further divided into K_1 contributed by H_1 , K_2 contributed by H_2 , and K_{21} contributed by their product,

$$[\mathbf{K}_{1}(\lambda d)]_{PQ} = \sum_{ar,a'r'} (P|ar)\lambda_{ar}d_{ar}[(aa'|rr') + (ar'|a'r)](a'r'|\mathbf{Q}|Q),$$
(44)

$$[\mathbf{K}_{2}(\lambda d)]_{PQ} = \sum_{ar,a'r'} (P|ar)\lambda_{ar}d_{ar}[(aa'|rr') - (ar'|a'r)](a'r'|\mathbf{Q}|Q),$$
(45)

$$[\mathbf{K}_{21}(\lambda)]_{PQ} = \sum_{ar,a'r',a''r''} (P|ar)\lambda_{ar}[(aa''|rr'') - (ar''|a''r)] \times [(a'a''|r'r'') - (a'r''|a''r')](a'r'|\mathbf{Q}|\mathbf{Q}), \quad (46)$$

and χ'_0 is the uncoupled FDDS "corrected" by removing the portion of ALDA exchange that is replaced by Hartree–Fock type exchange,

$$\chi_0' = \chi_0 - \xi \mathbf{K}_2'(\lambda), \tag{47}$$

$$[\mathbf{K}'_{2}(\lambda)]_{PQ} = \sum_{ar,a'r'} (P|ar)\lambda_{ar}[(aa'|rr') - (ar'|a'r)](a'r'|Q), \quad (48)$$

$$d_{ar} = \epsilon_r - \epsilon_a, \tag{49}$$

$$\lambda_{ar} = -\frac{4}{d_{ar}^2 + \omega^2},\tag{50}$$

where the 3-index tensor $(ar|\mathbf{Q}|Q)$ and matrix \mathbf{R} come from a QR factorization of the tensor (ar|Q) (as an $N_{occ}N_{vir} \times N_{aux}$ matrix). QR factorization decomposes any matrix into a product of an orthogonal matrix \mathbf{Q} and an upper triangular matrix \mathbf{R} . We needed the QR factorization here because the above equations originally include the pseudoinverse of (ar|Q), which has a relatively large condition number, and QR factorization of such a matrix helps avoid further condition problems when trying to invert it. In the above formulas, what actually appears is the pseudo-inverse of the transposed 3-index tensor (Q|ar),

$$(Q|ar) = (\mathbf{Q}\mathbf{R})^T = \mathbf{R}^T \mathbf{Q}^T, \tag{51}$$

$$[(Q|ar)]^{\dagger} = \mathbf{Q}(\mathbf{R}^T)^{-1}. \tag{52}$$

For hybrid functionals ($\xi \neq 0$), the most expensive part of the algorithm is computing the matrices with Hartree–Fock type exchange, i.e., \mathbf{K}_1 , \mathbf{K}_2 , \mathbf{K}_2' , \mathbf{K}_{21} , with a scaling of $O(N_{occ}^0 N_{vir}^0 N_{aux})$. For non-hybrid functionals, all these matrices vanish, and the scaling of the algorithm reduces to $O(N_{occ} N_{vir} N_{aux}^2)$. While Eqs. (44)–(46) seem to be very complicated, the above scaling can be achieved by storing the following intermediate 3-index tensors on the disk:

$$(ar|Y|Q) = [(a'r|ar') - (aa'|rr')](a'r'|Q),$$
 (53)

$$(ar|\mathbf{Q}_X|Q) = [(a'r|ar') + (aa'|rr')](a'r'|\mathbf{Q}|Q), \tag{54}$$

$$(ar|\mathbf{Q}_{v}|Q) = [(a'r|ar') - (aa'|rr')](a'r'|\mathbf{Q}|Q), \tag{55}$$

and the K matrices can be obtained from these intermediates,

$$[\mathbf{K}_{1}(\lambda d)]_{PQ} = -\xi \sum_{ar} (P|ar) \lambda_{ar} d_{ar} (ar|\mathbf{Q}_{X}|Q), \tag{56}$$

$$[\mathbf{K}_{2}(\lambda d)]_{PQ} = -\xi \sum_{ar} (P|ar) \lambda_{ar} d_{ar} (ar|\mathbf{Q}_{Y}|Q), \tag{57}$$

$$[\mathbf{K}_{21}(\lambda)]_{PQ} = \xi^2 \sum_{ar} (P|\mathbf{Y}|ar) \lambda_{ar} (ar|\mathbf{Q}_X|Q), \tag{58}$$

$$[\mathbf{K}_{2}'(\lambda)]_{PQ} = -\xi \sum_{ar} (P|ar) \lambda_{ar}(ar|\mathbf{Y}|Q). \tag{59}$$

D. Exchange-dispersion scaling

The computation of exchange-dispersion energy has been a challenge in SAPT(DFT). The uncoupled approximation has been unsatisfactory, and although Garcia *et al.*⁴⁶ resolved the problem of the requirement of the storage of 4-index TDDFT amplitudes on the disk when computing the coupled exchange-dispersion energy explicitly,³⁴ the coupled exchange-dispersion energy with hybrid kernel might be considerably more computationally demanding than the pure ALDA kernel case implemented by Garcia *et al.* Nevertheless, the solution provided by Garcia *et al.* is valuable, and we should pursue the implementation of the coupled exchange-dispersion term with hybrid kernel in the future. One way to avoid the explicit computation of coupled exchange-dispersion energy, proposed by Bukowski *et al.*,⁴⁰ is to estimate its value by scaling its uncoupled counterpart,

$$\tilde{E}_{\text{exch-disp, r}}^{(2)} = E_{\text{exch-disp, u}}^{(2)} \cdot \frac{E_{\text{disp, r}}^{(2)}}{E_{\text{disp, u}}^{(2)}}.$$
 (60)

This scaling scheme is straightforward but was shown by Hesselmann and Korona 34 to strongly underestimate the coupled exchange-dispersion energies for larger values according to results on the S22 \times 5 test set. 35 In the same paper, they proposed to scale the uncoupled exchange-dispersion energy by a fixed factor from linear fitting instead,

$$\tilde{E}_{\text{exch-disp, r}}^{(2)} = \alpha \cdot E_{\text{exch-disp, u}}^{(2)} (\alpha = 0.686361).$$
 (61)

From the results on S22 \times 5, the fixed factor scheme was shown extremely successful for estimating the coupled exchange-dispersion energies, with a mean absolute error of merely 0.03 kcal mol^{-1} as opposed to 0.19 kcal mol^{-1} for the conventional scaling scheme. However, these results are based on the local Hartree–Fock approximation for DFT calculations as proposed in Ref. 25. As we will demonstrate later, the uncoupled dispersion and exchange-dispersion energies would be heavily affected by the occupied-virtual orbital energy gap that appears in the denominator of the uncoupled dispersion amplitudes and differs between LHF and non-LHF algorithms significantly. Fortunately, the linear correlation between exact coupled exchange-dispersion energies and the non-LHF uncoupled values is still satisfactory, and thus, we are able to obtain a new scaling factor from linear fitting.

III. RESULTS

A. Exchange-dispersion scaling

As mentioned above, it is computationally costly to evaluate coupled exchange-dispersion energies with hybrid kernels, and so, we wish to estimate these terms by scaling the uncoupled exchange-dispersion energies. However, we cannot use existing scaling factors from the literature using LHF approaches because the difference in the occupied-virtual orbital energy gap between LHF and non-LHF approaches affects the uncoupled exchange-dispersion energies. We have plotted each SAPT(DFT) energy term calculated from LHF and non-LHF orbitals in Fig. 1 for the S66 test set.³⁶ In all SAPT(DFT) calculations in this section, we use the PBE0AC xc potential to

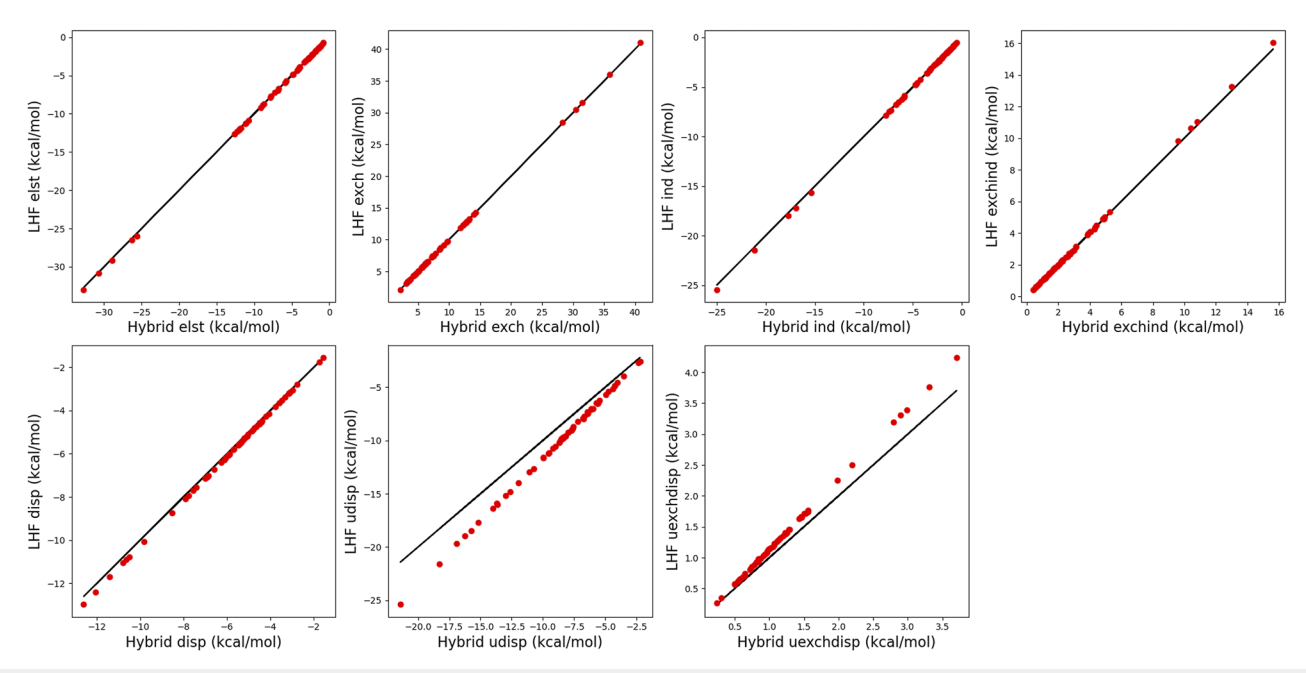


FIG. 1. LHF orbital/pure ALDA kernel (y-axis) vs non-LHF orbital/hybrid ALDA kernel (x-axis) SAPT(DFT) components for S66 dimers with the aug-cc-pVTZ basis set. All energies are in units of kcal mol⁻¹. The components plotted are from top-left to bottom-right: electrostatics, exchange, induction, exchange-induction, coupled dispersion, uncoupled dispersion, and uncoupled exchange-dispersion.

generate the Kohn–Sham orbitals, except for calculations adopting the LHF approach, where the exact exchange of PBE0AC would be localized with LHF as described in Ref. 25, and we use the augmented version of the correlation-consistent basis sets of Dunning and co-workers, aug-cc-pVDZ and aug-cc-pVTZ. 47,48

The plots show that while the first-order and induction terms are almost unaffected by the LHF orbitals, the uncoupled dispersion and exchange-dispersion energies are substantially affected. Nevertheless, it is fortunate that the uncoupled terms between LHF and non-LHF orbitals seem to approximately follow a linear relationship, which would be very helpful for us to build up our scaling scheme for the exchange-dispersion energy. It is also worth mentioning that although computed from totally different algorithms, the coupled dispersion energies from the non-LHF potential combined with a hybrid ALDA kernel turn out to be almost identical to their LHF potential/pure ALDA kernel counterparts. From these results, we can safely conclude that we can perform another linear fitting to obtain a new scaling factor appropriate for scaling uncoupled exchange energies computed with non-LHF orbitals.

We perform a linear fit between LHF orbital/pure ALDA kernel coupled exchange-dispersion energies and non-LHF orbital/hybrid ALDA kernel uncoupled exchange-dispersion energies for the S22 \times 5 test set. As expected, we are able to establish a linear correlation here, given by the following expression:

$$E_{\text{exch-disp}}^{(2)}(\text{coupled}) \approx \alpha \cdot E_{\text{exch-disp}}^{(2)}(\text{uncoupled})(\alpha = 0.770).$$
 (62)

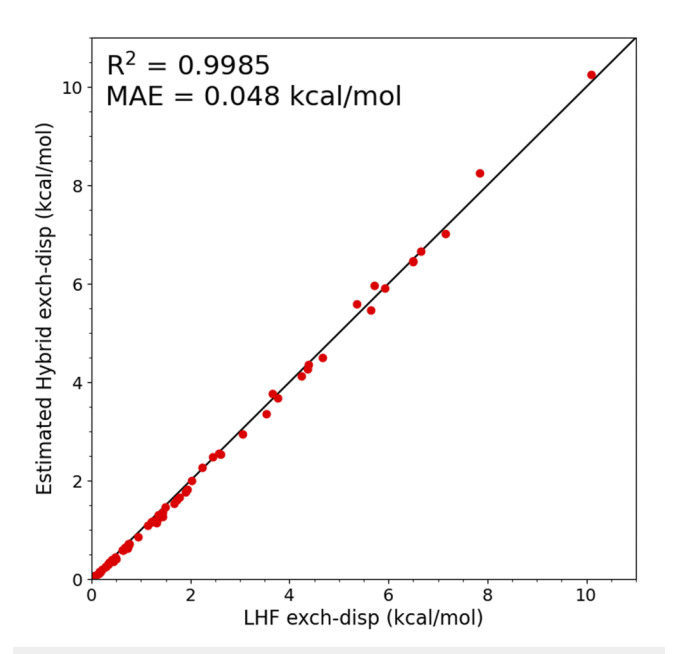


FIG. 2. Exchange-dispersion fitting results for the S22 \times 5 complexes with the aug-cc-pVTZ basis set. The estimated coupled, non-LHF orbital/hybrid ALDA kernel exchange-dispersion energies from Eq. (62) (y-axis) are plotted against the coupled, LHF orbital/pure ALDA kernel exchange-dispersion energies (x-axis) computed with Molpro.

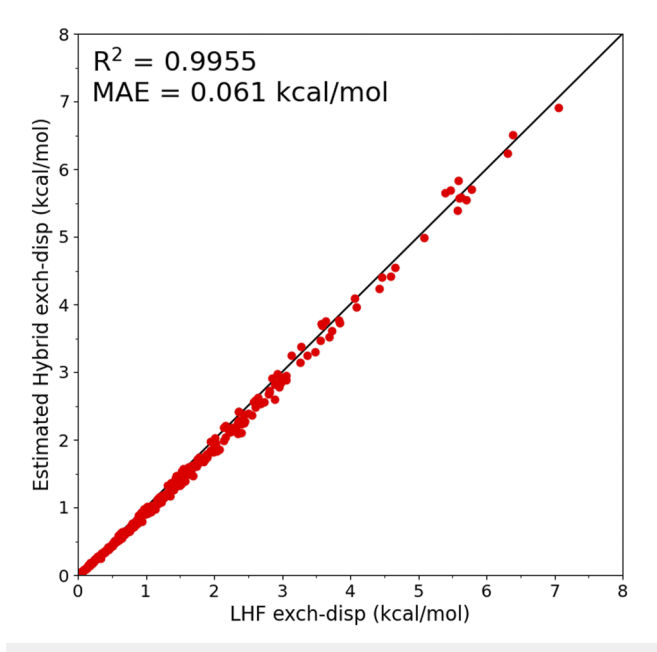


FIG. 3. Exchange-dispersion fitting results for the S66 \times 8 complexes with the aug-cc-pVTZ basis set. The estimated coupled, non-LHF orbital/hybrid ALDA kernel exchange-dispersion energies from Eq. (62) (y-axis) are plotted against the coupled, LHF orbital/pure ALDA kernel exchange-dispersion energies (x-axis) computed with Molpro.

The mean absolute error of the estimated coupled exchange-dispersion energy is 0.048 kcal mol $^{-1}$, and the correlation coefficient of the linear fitting is 0.9985 (Fig. 2). While not quite as good as the results (0.03 kcal mol $^{-1}$ and 0.9993) in Ref. 34, this fit is still satisfactory for the purpose of estimating the exchange-dispersion energy in SAPT(DFT). In order to validate the scaling scheme, we scale the uncoupled exchange-dispersion energies of S66 \times 8 with the fitted scaling factor of 0.770 from S22 \times 5 and compare with the reference values from the LHF approach. This estimation has a mean absolute error of 0.061 kcal mol $^{-1}$ and a correlation coefficient of 0.9955 (Fig. 3). These results suggest that this scaling scheme should suffice for estimating exchange-dispersion energies in SAPT(DFT) with hybrid functionals when LHF is not used.

B. Accuracy of SAPT(DFT) interaction energy

To assess the accuracy of term-wise and total interaction energies of SAPT(DFT), we compare to benchmark results. For energy components (exchange, electrostatics, induction, and dispersion), SAPT based on CCSD monomer wavefunctions, i.e., SAPT(CCSD), should provide good reference values. 49 Compared to many-body perturbation theory based SAPT, this approach avoids potential poor or oscillatory convergence with respect to the perturbation order of the intramolecular correlation. Unfortunately, SAPT(CCSD) is very computationally costly, and the published SAPT(CCSD) results are only available for a limited set of systems containing no more than 10 atoms. 49 We compare SAPT(DFT) energy components to the available SAPT(CCSD) energy components below.

In order to examine a larger test set that is more inclusive of common types of intermolecular interactions, we also compare SAPT(DFT) energy components to those from the more computationally tractable SAPT2+3(CCD) δ MP2 approach⁵⁰ for the S66 set of van der Waals dimers.^{37,38} This method is a many-body perturbation theory approach to SAPT although it utilizes coupled-cluster theory for dispersion [in particular, the CCSD+ST(CCD) approach of Williams *et al.*].⁵¹ It has the potential advantage over SAPT(CCSD) that certain terms are included through the third order in the intermolecular perturbation \hat{V} , and certain higher-order terms (mainly induction-like) are implicitly included through the " δ MP2" correction, which is a generalization of the δ HF correction commonly used in SAPT.⁵⁰ Total energies computed with this approach have been found to be quite accurate in comparison with CCSD(T).⁵⁰

1. SAPT(CCSD) reference

In order to assess the performance of our hybrid-kernel SAPT(DFT) scheme, we compare the results of several SAPT schemes using SAPT(CCSD) as the reference for each component. As mentioned above, SAPT(CCSD) results are only available for a limited set of small systems; here, we use published SAPT(CCSD)/aug-cc-pVTZ results for a set of 14 dimers named S2 by Korona. Our comparison includes our implementation of hybrid-kernel SAPT(DFT) in PSI4 and LHF-orbital SAPT(DFT) as implemented in Molpro, both using the aug-cc-pVTZ basis set, and SAPT0 with the aug-cc-pVDZ basis set (SAPT0 has better error cancellation for total interaction energies when used with basis sets of this size.

In addition, in order to apply the GRAC scheme, one needs to know the highest occupied orbital eigenvalue and the ionization potential of both monomers in each dimer. In our work, the HOMO eigenvalues are obtained by running a DFT calculation with the plain PBE0 functional and aug-cc-pVTZ basis set, and the ionization potentials for Korona S2 systems are obtained from the original work of Korona.⁴⁹

The results for the S2 test set are presented in Table I. Both the mean absolute error (MAE) and the mean unsigned error (MURE) with respect to SAPT(CCSD) are presented because of the existence of strongly interacting systems in S2 (e.g., HF dimer) that might skew the statistics of absolute errors. In addition to the statistics, strip charts are included in this table as a visual representation of errors from all database members. Each vertical line in the chart represents the error (in kcal mol⁻¹) of the SAPT term of interest for a dimer in S2 with respect to SAPT(CCSD)/aug-cc-pVTZ on either the overbound (-) or the underbound (+) side, and a black rectangular marker (always on the overbound side) is used to indicate the mean absolute error over S2 of the given SAPT term and theory lovel.

The mean absolute error of the total interaction energy and every SAPT term is below 0.2 kcal mol⁻¹ for hybrid-kernel SAPT(DFT) and LHF-orbital SAPT(DFT), with the exception of exchange energies. The mean unsigned relative errors for these two approaches are also below 5% for the total interaction energy and all components, with the exception of the exchange-dispersion term

of hybrid-kernel SAPT(DFT), which has a mean unsigned relative error of 12.47%. Nevertheless, because of the small magnitude of the exchange-dispersion term, the mean absolute error of hybrid-kernel SAPT(DFT) for this term remains only 0.062 kcal mol⁻¹, meaning that this error has only a very small effect on the overall dispersion interaction or the total interaction energy.

For the S2 test set, hybrid-kernel SAPT(DFT)/aug-cc-pVTZ and LHF-orbital SAPT(DFT)/aug-cc-pVTZ show significantly improved accuracy vs SAPT0/aug-cc-pVDZ when compared to SAPT(CCSD)/aug-cc-pVTZ benchmark components and total energies. This is consistent with our previous findings for SAPT(DFT)/aug-cc-pVTZ vs SAPT0/aug-cc-pVDZ for total interaction energies for the S22, NBC10, HBC6, and HSG test sets. ⁵⁰ The mean absolute errors for the exchange, induction, and exchange-induction terms for SAPT0 are larger than 1 kcal mol⁻¹, i.e., larger than "chemical accuracy." The mean absolute error in the total interaction energy is also slightly over 1 kcal mol⁻¹, which is comparable to its mean absolute errors for some other test sets. ⁵⁰

The results for dispersion in Table I show a drawback of what we have labeled the "non-hybrid" SAPT(DFT) approach, i.e., computing the dispersion energy using a hybrid functional and pure ALDA kernel directly (as if one would do with a non-hybrid functional); this approach has a mean absolute error of 0.326 kcal mol⁻¹ and a mean unsigned relative error of 9.58% in the dispersion term, which is less satisfactory compared to 0.175 kcal mol⁻¹ and 3.68% for hybrid-kernel SAPT(DFT) and 0.141 kcal mol⁻¹ and 2.77% for LHF SAPT(DFT). From the strip chart, we can observe that all SAPT(DFT) approaches underbind the dispersion interactions in S2, and the "non-hybrid" approach underbinds them to a larger extent. This systematic error introduced by the combination of hybrid xc potential and pure ALDA xc kernel was discussed in Ref. 25, which points out that the hybrid xc potential broadens the occupied-virtual orbital energy gaps and thus lowers the magnitude of dispersion energies. In general, the SAPT(CCSD) results of Korona S2 are fairly accurately reproduced with both SAPT(DFT) approaches that have a proper treatment for the hybrid DFT functional, namely, a hybrid ALDA kernel or a LHF variation in the xc potential. The mean absolute error for the dispersion term is roughly doubled for "nonhybrid" SAPT(DFT) although it remains modest at a third of one kcal mol⁻¹, and error cancellation for this test set leaves the MAE for total interaction energies only slightly elevated (0.244 kcal mol⁻¹) vs hybrid-kernel SAPT(DFT) and LHF-orbital SAPT(DFT) (0.155 and 0.189 kcal mol⁻¹, respectively). "Non-hybrid" SAPT(DFT) remains a significant improvement over SAPT0/aug-cc-pVDZ for this test set.

For the interested reader, Table S1 in the supplementary material provides a comparison of SAPT2+3(CCD) δ MP2 vs SAPT(CCSD), both in the aug-cc-pVTZ basis, for the Korona S2 test set. Differences between these two high-level SAPT treatments can be taken as a measure of the approximate accuracy of each approach. As mentioned above, SAPT(CCSD) and SAPT2+3(CCD) δ MP2 have accuracy advantages and disadvantages relative to each other. Table S1 shows that across all energy components, and the total interaction energy, the great majority of the S2 systems show differences of less than 0.3 kcal mol⁻¹, with occasional outliers. Mean absolute deviations between the methods are 0.1–0.2 kcal mol⁻¹ for components and slightly larger for the overall interaction energy (0.32 kcal mol⁻¹). Compared to these differences, the SAPT(DFT)

TABLE I. Mean absolute errors (kcal mol⁻¹) and mean unsigned relative errors (%) of the interaction energy components for the Korona S2 test set with various SAPT methods.

				Erro	or distribution ^b		
Method ^a	MAE	MURE	4	OB 1	0 1	UB	4
Electrostatics							
SAPT(DFT) hybrid	0.112	2.39					
SAPT(DFT) LHF	0.114	3.69					
SAPT0	0.520	8.61	ļ	1			
		Exchange					
SAPT(DFT) hybrid	0.251	3.38					
SAPT(DFT) LHF	0.258	3.09					
SAPT0	1.757	12.88					
Induction							
SAPT(DFT) hybrid	0.148	2.79					
SAPT(DFT) LHF	0.192	2.97				1	
SAPT0	1.993	16.83			[], [] []]		
Exchange-induction							
SAPT(DFT) hybrid	0.144	4.03					
SAPT(DFT) LHF	0.165	4.76					
SAPT0	1.551	26.80					
Dispersion							
SAPT(DFT) hybrid	0.175	3.68					
SAPT(DFT) LHF	0.141	2.77		[
SAPT(DFT) non-hybrid	0.326	9.58					
SAPT0	0.811	24.86		I			
Exchange-dispersion							
SAPT(DFT) hybrid	0.062	12.47					
SAPT(DFT) LHF	0.039	3.25					
SAPT0	0.265	36.11					
Total							
SAPT(DFT) hybrid	0.155	4.98					
SAPT(DFT) LHF	0.189	4.17					
SAPT(DFT) non-hybrid	0.244	10.64					
SAPT0	1.237	19.63	1 1	1			

^a All SAPT(DFT) results use the PBE0AC functional and the aug-cc-pVTZ basis set. Hybrid denotes the use of the hybrid ALDA kernel, non-hybrid denotes the use of the pure ALDA kernel, and LHF denotes the use of the local Hartree–Fock functional fit to the PBE0AC functional and the pure ALDA kernel. SAPT0 results use the aug-cc-pVDZ basis set.

^b Errors with respect to SAPT(CCSD)/aug-cc-pVTZ. Each vertical line indicates the error for a member of S2 on either the overbound (+) or the underbound (−) side of the middle bar. Errors with an absolute value greater than 4 kcal mol⁻¹ are plotted at the edge of the spectrum, separated by an interval of 0.05 kcal mol⁻¹. The mean absolute error of each term (in kcal mol⁻¹) over the whole S2 set is marked by a black rectangular marker on the overbound side. Guidelines are at 0, 0.3, and 1.0 kcal mol⁻¹ overbound and underbound.

hybrid and SAPT(DFT) LHF are in extremely good agreement with each other for S2, and on average, their errors vs SAPT(CCSD) are similar to the differences between SAPT(CCSD) and SAPT2+3(CCD) δ MP2.

2. SAPT2+3(CCD) δMP2 reference

To investigate more completely, we compare to the larger S66 test set; 36 here, SAPT2+3(CCD) δ MP2 values are used as the

TABLE II. Mean absolute error (kcal mol⁻¹) of the interaction energy for S66 with various SAPT methods.

					Error distribution ^b
Method ^a	Total	НВ	MX	DD	4 OB 1 0 1 UB 4
Electrostatics					
SAPT(DFT) hybrid	0.374	0.556	0.177	0.331	
SAPT(DFT) LHF	0.423	0.666	0.196	0.319	
SAPT0	0.613	1.034	0.439	0.297	
SAPT2+	0.236	0.270	0.136	0.263	••••••
SAPT2+(3)δMP2	0.000	0.000	0.000	0.000	
Exchange					
SAPT(DFT) hybrid	0.866	1.127	0.426	0.926	u i i i i i i i i i i i i i i i i i i i
SAPT(DFT) LHF	0.866	1.121	0.431	0.928	11 II I
SAPT0	0.675	0.942	0.263	0.658	
SAPT2+	0.337	0.467	0.277	0.277	
SAPT2+(3)δMP2	0.000	0.000	0.000	0.000	
Induction					
SAPT(DFT) hybrid	0.211	0.201	0.212	0.220	
SAPT(DFT) LHF	0.224	0.223	0.223	0.225	[
SAPT0	0.241	0.200	0.261	0.271	" """
SAPT2+	0.327	0.384	0.250	0.318	1 11101
SAPT2+(3)δMP2	0.152	0.179	0.121	0.145	1 200
Dispersion					
SAPT(DFT) hybrid	0.370	0.260	0.219	0.573	[■ (100) (10) (10)
SAPT(DFT) LHF	0.308	0.200	0.173	0.499	
SAPT(DFT) non-hybrid	0 635	0.581	0.419	0.822	 1/10/1 000 1/1 1/
SAPT0	0.443	0.862	0.162	0.195	
SAPT2+	0.235	0.397	0.169	0.115	i iiiii i
SAPT2+(3)δMP2	0.093	0.129	0.056	0.080	
Total					
SAPT(DFT) hybrid	0.334	0.588	0.107	0.217	III III III
SAPT(DFT) LHF	0.234	0.382	0.046	0.199	III
SAPT(DFT) non-hybrid	0.604	0.955	0.389	0.385	
SAPT0	0.990	1.197	0.692	0.965	
SAPT2+	0.230	0.235	0.138	0.280	
SAPT2+(3) δ MP2	0.105	0.056	0.082	0.169	

a All SAPT(DFT) results use the PBE0AC functional and the aug-cc-pVTZ basis set. Hybrid denotes the use of the hybrid ALDA kernel, non-hybrid denotes the use of the pure ALDA kernel, and LHF denotes the use of the local Hartree–Fock functional fit to the PBE0AC functional and the pure ALDA kernel. SAPT0 and SAPT2+ results use the aug-cc-pVDZ basis set; SAPT2+(3)δMP2 results use the aug-cc-pVTZ basis set.

b Errors with respect to SAPT2+3(CCD) δ MP2/aug-cc-pVTZ. Each vertical line indicates the error for a member of S66 on either the overbound (+) or the underbound (-) side of the middle bar. Errors with an absolute value greater than 4 kcal mol⁻¹ are plotted at the edge of the spectrum, separated by an interval of 0.05 kcal mol⁻¹. The color of the line indicates the category of the system: hydrogen-bonded (HB, red), mixed-influence (MX, green), or dispersion-dominated (DD, blue). The mean absolute error of each term (in kcal mol⁻¹) over the whole S66 set is marked by a black rectangular marker on the overbound side. Guidelines are at 0, 0.3, and 1.0 kcal mol⁻¹ overbound and underbound.

reference. As before, we compare three approaches to SAPT(DFT) and also the least computationally expensive version of SAPT, SAPT0. We also include the "silver standard" SAPT2+/aug-cc-pVDZ and "gold standard" SAPT2+(3)δMP2, which are Pauling points of SAPT theory as shown in Ref. 50. Direct comparisons against SAPT0 and SAPT2+ in the aug-cc-pVTZ basis, which generally provide poorer error cancellation for those levels of SAPT, are provided in the supplementary material. The ionization potentials of molecules needed for SAPT(DFT) calculations are computed from the energy of each molecule and its +1 cation using the PBE0 functional and the def2-TZVPP basis set.⁵³

In S66, the dimers are divided into 3 subsets by dominating contributions to the interaction: 23 dimers dominated by electrostatic interactions, typically hydrogen-bonding (HB); 23 dispersion-dominated interactions (DD); and 20 mixed-influence (MX) dimers. Mean absolute errors for energy components and total interaction energies are presented in Table II for S66 overall and also for each subset (HB, MX, and DD). Similar to Table I, strip charts show error distributions, and in this case, lines for each error are color coded for the dominant interaction type in each dimer: red for HB, green for MX, and blue for DD.

As shown in Table II, the mean absolute errors over S66 for SAPT(DFT) with the PBE0AC functional and the aug-cc-pVTZ basis set are 0.334 (hybrid kernel), 0.234 (LHF orbitals with ALDA kernel), and 0.604 kcal mol⁻¹ (non-hybrid pure ALDA kernel). The close agreement between the hybrid kernel and LHF approaches mimics that seen for S2 and persists for both for mean absolute errors and error distributions. The larger error for the non-hybrid approach is also consistent with the results for S2 although the differences are magnified here for the S66 test set, which includes larger molecules. The non-hybrid SAPT(DFT) dispersion is almost always underbound (consistent with the S2 results), whereas the hybrid kernel and LHF approaches are somewhat more balanced in their error distributions. With the exception of the dispersion-dominated complexes, mean absolute errors for dispersion are almost twice as large for non-hybrid SAPT(DFT) vs hybrid kernel or LHF-based SAPT(DFT).

All three SAPT(DFT) approaches considered here provide an improvement in the MAE compared to 0.990 kcal mol⁻¹ for SAPT0/aug-cc-pVDZ. For S66, SAPT0 is nearly always overbound, whereas the behavior of SAPT(DFT) is somewhat more balanced (although the majority of the complexes are underbound). Both the hybrid-kernel and LHF-orbital SAPT(DFT) approaches provide similar MAEs overall and across subsets compared to the computationally expensive SAPT2+/aug-cc-pVDZ approach that has an MAE across S66 of 0.230 kcal mol⁻¹. However, MAEs for the hybridkernel and LHF-based SAPT(DFT) are somewhat worse than those for SAPT2+ for the hydrogen-bonded subset, and error distributions across S66 are wider for SAPT(DFT) compared to SAPT2+. Errors for total interaction energies and their components are much smaller for high-level SAPT2+(3)δMP2/aug-cc-pVTZ, with an overall MAE across S66 of only 0.105 kcal mol⁻¹. Our findings for errors in total interaction energies of S66 for the LHF-orbital SAPT(DFT), SAPT0, SAPT2+, and SAPT2+(3) δ MP2 methods are in qualitative agreement with our previous study of errors in total interaction energies for the S22, NBC10, HBC6, and HSG test sets.

Regarding energy components, SAPT(DFT) and SAPT0 exhibit roughly similar error distributions for electrostatics, with

hydrogen-bonded systems tending to be overbound and with dispersion-dominated dimers having their error distribution shifted a little toward the underbound side. Overall, SAPT(DFT) is more reliable than SAPTO on average for electrostatics, especially for H-bonded systems, where there are several significantly overbound systems with SAPT0. For dispersion-dominated complexes, SAPT(DFT) performs similarly to SAPT0 for electrostatics. Errors for induction are quite similar for SAPT0, SAPT(DFT), and SAPT2+. For dispersion energies, SAPT0 tends to underbind hydrogen-bonded complexes (sometimes significantly) and slightly overbinds dispersion-dominated complexes. SAPT(DFT) with the hybrid kernel or LHF orbitals, by contrast, shows some underbound dispersion-dominated complexes and a few overbound H-bonded complexes. On average, hybrid-kernel or LHF-based SAPT(DFT) is more accurate than SAPT0 for dispersion, especially for H-bonded complexes; the errors for the dispersion-dominated subset are slightly larger for SAPT(DFT) than for SAPT0 (perhaps due to a favorable error cancellation between the simple treatment of dispersion in SAPT0 and the modest aug-cc-pVDZ basis set used here for SAPT0). As pointed out above, the "non-hybrid" approach to SAPT(DFT) exhibits larger MAEs for dispersion than hybrid kernel or LHF-based SAPT(DFT), and it is generally worse than SAPT0 except for a slight improvement for the H-bonded subset. For the exchange term, SAPT(DFT) shows a wide range of errors, spanning the entire ± 1 kcal mol⁻¹ range, with several larger errors on the overbound side for dispersion-dominated dimers and several larger errors on the underbound side, generally hydrogen-bonded. The SAPT0 error distribution is compressed and shifted toward the overbound side, and it exhibits more strongly overbound outliers (now more frequently of the hydrogen-bonding type). The overall MAE for exchange is somewhat similar for SAPT0 and SAPT(DFT).

In summary, SAPT(DFT) with the PBE0AC functional and the aug-cc-pVTZ basis set performs similarly across total interaction energies and their components whether we use the LHF-orbital formulation or the hybrid kernel, and in general, interaction energies and their components are superior to those from SAPT0, except for the exchange component. SAPT(DFT) results for total interaction energies have similar MAEs as the computationally much more expensive SAPT2+ wavefunction-based SAPT although the error distribution is wider for SAPT(DFT). Similarly, energy components from SAPT(DFT) are often of roughly similar quality as SAPT2+ on average (although larger errors are seen for exchange energies), but the error distributions are wider. Using SAPT(DFT) with the PBE0AC functional but without either the hybrid kernel or an LHF-orbital approach creates larger errors in the dispersion term and the overall interaction energy; this approach remains more accurate on average than SAPT0 but is no longer competitive with SAPT2+ in accuracy.

C. Timing performance

In order to investigate the efficiency of our hybrid kernel dispersion algorithm and our overall SAPT(DFT) implementation, we obtained run-times for the Watson–Crick adenine–thymine complex (WCAT) and the RDX dimer using different numbers of cores (1, 2, 4, and 6) on an Intel Core i7-6800K processor (6 cores, 3.4 GHz) with 128 GB RAM. The geometry of adenine–thymine is

obtained from the S22 test set⁵⁴ and the RDX dimer from Ref. 40. The aug-cc-pVDZ and aug-cc-pVTZ basis sets are used for both systems. Below, we will also discuss timings for the C_{60} -buckycatcher complex using an aug-cc-pVDZ basis set. The testing systems in this section are shown in Fig. 4, and the number of basis functions (N_{bf}) , occupied orbitals (N_{occ}) , virtual orbitals (N_{vir}) , and auxiliary functions (N_{aux}) of each combination of the dimer system and basis set is listed in Table III.

Timings results of the WCAT and RDX dimer are presented in Fig. 5, showing the breakdown of the timing data by the module for the test systems using 6 cores. The entire SAPT(DFT) computation is divided into 6 modules as follows:

1. "Delta HF" for the computations related to evaluating the δ HF term, ²⁵ including HF calculations of the dimer and monomer and a SAPT0 calculation of electrostatics, exchange, and induction terms.

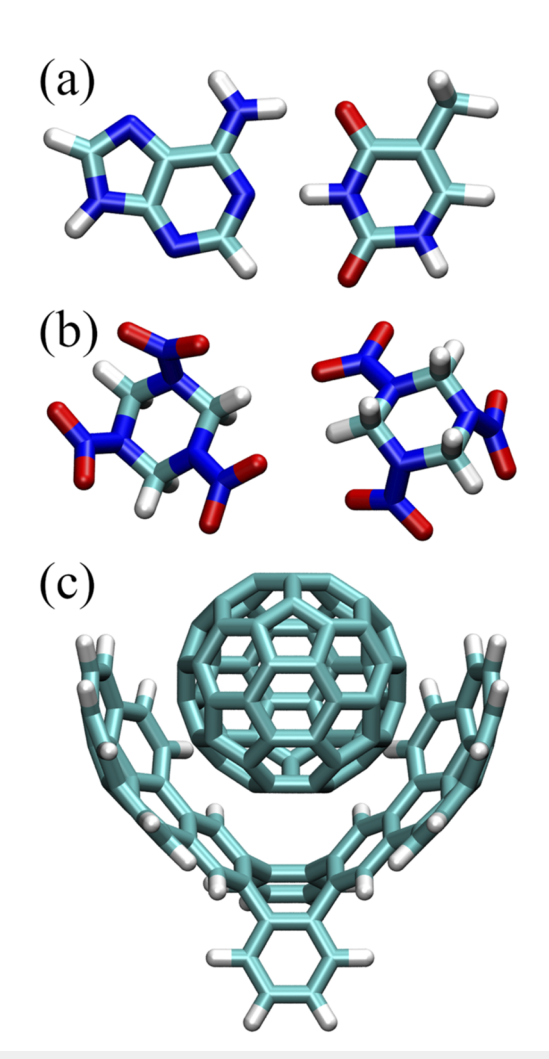


FIG. 4. Dimer systems tested for program runtime performance: (a) Watson–Crick adenine–thymine complex, (b) RDX dimer, and (c) C_{60} –buckycatcher complex.

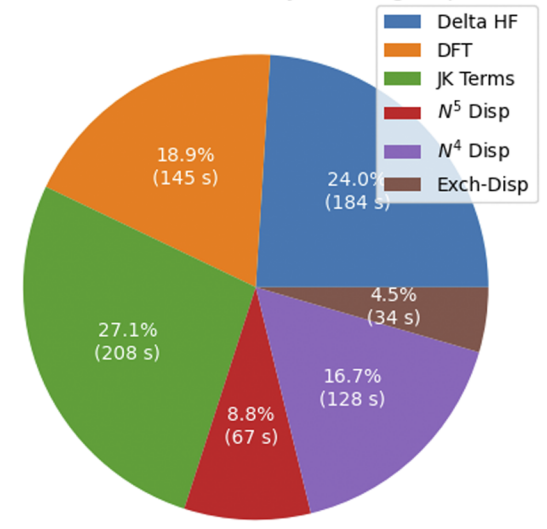
TABLE III. Number of basis functions (N_{bf}) , occupied orbitals (N_{occ}) , virtual orbitals (N_{vir}) , and auxiliary functions (N_{aux}) for different systems and basis sets.

	Adenine-thymine		RDX	dimer	Buckycatcher	
System size	aDZ	aTZ	aDZ	aTZ	aDZ	
$\overline{N_{bf}}$	536	1127	798	1656	3012	
$N_{occ,A}$	35	35	57	57	180	
$N_{vir,A}$	501	1092	741	1599	2832	
$N_{occ,B}$	33	33	57	57	194	
$N_{vir,B}$	503	1094	741	1599	2818	
N_{aux}	1621	2520	2436	3732	9284	

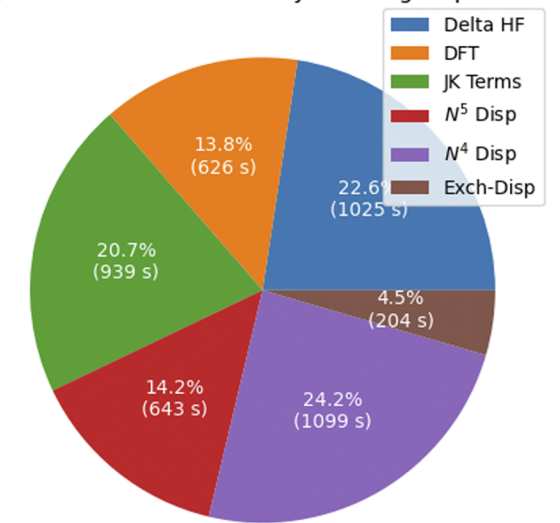
- 2. "DFT" for the DFT calculation of both monomers in order to obtain the Kohn–Sham orbitals.
- "JK terms" for electrostatics, exchange, induction, and exchange-induction terms, all of which are computed from certain generalized Coulomb (J) and exchange (K) matrices. Induction and exchange-induction take nearly all of the time for the JK terms (more than 90% for these test cases).
- 4. " N^5 Disp" for the $O(N^5)$ steps in the dispersion term, namely, the frequency-independent parts of Eqs. (44)–(48).
- 5. " N^4 Disp" for everything in the dispersion term aside from " N^5 Disp." This mainly includes the integration over ω as in Eq. (32) and the integral transformation step that involves the most disk I/O operations.
- "Exch-Disp" for the exchange-dispersion term as described in Subsection II D. This module also scales as O(N⁵) like "N⁵ Disp."

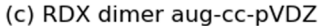
For our RDX and WCAT test cases, one would hardly claim that the $O(N^5)$ modules contribute dominantly to the total computational time. The "Exch-Disp" module takes up less than 10% of the total wall time, while the percentage of "N⁵ Disp" varies from 8.8% to 23.4% for different system sizes. The timings are distributed somewhat evenly between each module for all test cases; every block, from "Delta HF" to "N⁴ Disp," takes a considerable portion of the total wall time for these test cases. This suggests that the $O(N^5)$ scaling is not a major concern in SAPT(DFT) calculations of systems below 2000 basis functions; the total computational cost is more affected by iterative steps with lower formal scaling, including SCF calculations, CPKS calculations in the induction terms, and integration over ω . The fraction taken by the "N⁵ Disp" block of the total wall time also indicates the computational cost that could be saved if one would use the "non-hybrid" approach as indicated in Subsection III B 1. From the results in Subsections III B 1 and III B 2, the improvement in the accuracies of dispersion energies and total interaction energies introduced the hybrid-kernel algorithm is significant enough to justify the additional computational cost from the "N⁵ Disp" block. It is also interesting to note that these $O(N^5)$ blocks take a larger fraction of the total job wall time in the RDX dimer/aug-cc-pVDZ than in the WCAT/aug-cc-pVTZ even though the former does not have as many basis functions as the latter; this is partly because the detailed scaling of the $O(N^5)$ terms is $O(N_{occ}^2 N_{vir}^2 N_{aux})$, and the number of occupied orbitals for the RDX dimer/aug-cc-pVDZ is almost twice of that for the WCAT/aug-cc-pVTZ, while N_{vir} and N_{aux} change by a smaller ratio.

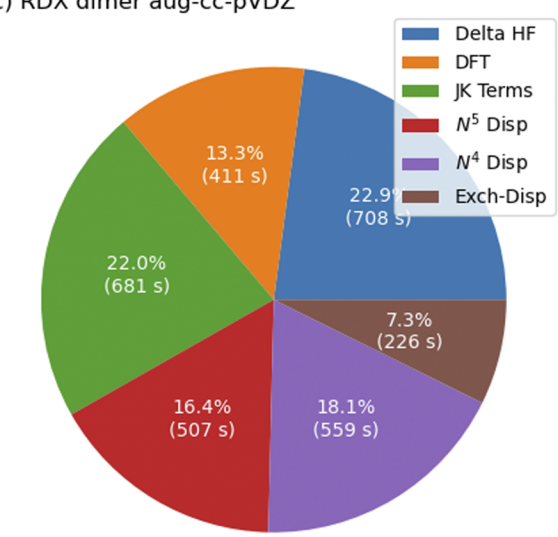
(a) Watson-Crick Adenine-Thymine aug-cc-pVDZ



(b) Watson-Crick Adenine-Thymine aug-cc-pVTZ







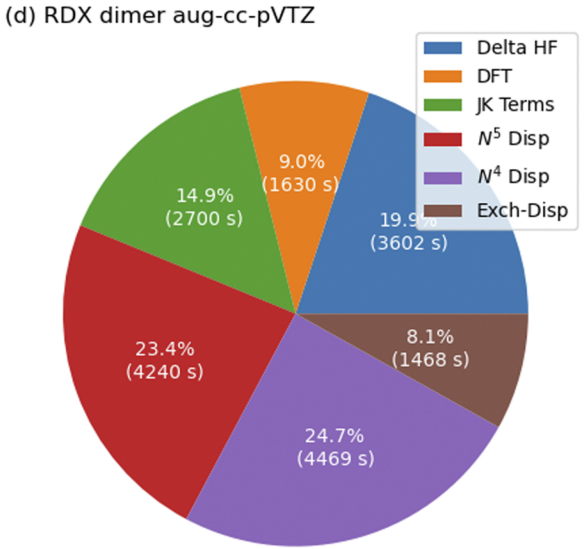


FIG. 5. (a)–(d) Distribution of wall time among subroutines for each test system with aug-cc-pVDZ and aug-cc-pVTZ basis sets with 6 cores.

Our timing results affirm the utility of the hybrid-kernel algorithm as an alternative to the LHF algorithm even though the former scales formally as $O(N^5)$ and the latter as $O(N^4)$ because the LHF algorithm will have a much larger prefactor. Although we have not implemented the LHF algorithm ourselves, we can obtain a more detailed comparison by performing test computations with the current hybrid kernel algorithm and the LHF algorithm implemented in the Molpro program package.⁵² We present the results of this comparison for the RDX dimer in the aug-cc-pVTZ basis in

Table IV. Here, the LHF algorithm takes 12.80 h with 6 cores, while the hybrid algorithm implemented in this work only takes a total wall time of 5.03 h. The DFT calculation with the LHF algorithm takes 2.29 h, which is about 5× slower than the hybrid algorithm, where a regular DFT calculation without LHF approximation is performed. The regular DFT calculation took 13 iterations to converge for both monomers, while the LHF-DFT calculation took 19 and 43 iterations, respectively, and this implies that the LHF approach might present some hindrance to the convergence of the

TABLE IV. Wall times (in hours) for SAPT(DFT) computations of the RDX dimer/ aug-cc-pVTZ with hybrid and LHF algorithms.

Subroutine	Hybrid	LHF
Delta HF	0.96	N/Aª
DFT	0.45	2.29
xc kernel	0.08	4.17
FDDS object ^b	2.35	N/A
Disp time integration	0.37	3.59
Exch-disp	0.41	1.99
Total	5.03	12.80

 $^{^{\}rm a}$ The δ HF correction, recommended for SAPT(DFT) computations of polar molecules, is performed by default in PS14 but not in Molpro.

SCF procedure. In addition, the Molpro program has not implemented a 2-index representation of the xc kernel as of version 2019.2 tested here, and the formation of the xc kernel costs a significant amount of time with the 3-index representation. The time integration part involves contractions between the xc kernel and other tensors, so it is also affected by the 3-index representation of the kernel. For the subroutines that are exclusive to the hybrid kernel algorithm, including the $O(N^5)$ part, the total wall time is only 2.35 h, only slightly longer than the cost introduced in DFT by the LHF approximation, so we may conclude that even if we do not consider the difference between 2-index and 3-index representations of the xc kernel, the $O(N^5)$ hybrid kernel algorithm would have an advantage for systems around the size of the RDX dimer with the aug-cc-pVTZ basis or smaller.

We also performed PBE0AC SAPT(DFT) computations with the hybrid kernel on the C₆₀-buckycatcher complex using the aug-cc-pVDZ basis set. The numbers of occupied and virtual orbitals are listed in Table III along with the previous test systems. The geometry of the complex was taken from Ref. 55 (complex C60@2). Because of the large size of the system, we used a more powerful computer for our timings tests, namely, an 18-core Intel Core i9-10980XE processor at 3.0 GHz, with 256 GB of RAM and a scratch disk array of three 7200 rpm disk drives in the RAID0 configuration. The wall time of the entire calculation was 4.03 days, and the detailed timing information is shown in Table V. For this system with 3012 basis functions, the $O(N^5)$ contributions to the dispersion term become more significant than in the previous test cases, and overall, the dispersion component is now the most time-consuming step (although followed closely by the time required to compute δ_{HF}).

The integral transformation procedure in the dispersion term is quite expensive, comparable to the $O(N^5)$ terms, and this can be attributed to the disk operation required for writing large 3-index integrals of form (rr'|Q), which are later used to reform the 4-index MO integral of form (aa'|rr') as in Eqs. (44)–(48).

In fact, this calculation was also performed in Ref. 56 with a non-hybrid DFT functional (HCTH407) and pure ALDA kernel, which allows the dispersion term to scale as $O(N^4)$ in contrast to the case of hybrid xc-kernel of $O(N^5)$. That work accomplished the same calculation with less computational cost than that reported

TABLE V. Wall times (in hours) for PBE0AC SAPT(DFT) computations of the C_{60} -buckycatcher complex using 18 cores of an Intel i9-10980XE processor with the hybrid algorithm.

Subroutine	Wall time
Delta HF	29.1
Dimer HF	6.3
C60 HF	6.2
Buckycatcher HF	6.6
Prepare JK	0.5
Exchange	0.5
Induction	8.9
DFT	14.8
C60 DFT	7.1
Buckycatcher DFT	7.7
JK terms	10.0
Prepare JK	0.5
Exchange	0.5
Induction	8.9
Dispersion	42.7
Transformation	10.5
QR factorization	0.5
Form X	7.0
Form Y	13.1
Time integration	4.3
Exchange-dispersion	6.8

here because of the avoidance of the $O(N^5)$ terms with the non-hybrid functional (and likely also omitting the δ_{HF} step). Using a non-hybrid functional is an effective approach when trying to perform SAPT(DFT) calculations for large systems with limited computation resources, but our computation demonstrates that even the hybrid xc-kernel variant of SAPT(DFT) is now able to handle systems with around 3000 basis functions.

IV. CONCLUSION

We have reported an implementation of symmetry-adapted perturbation theory based on a density functional theory description of the monomers, i.e., SAPT(DFT), ^{21,25,40} in the PSI4 open-source quantum chemistry program.³⁹ Hybrid functionals have become preferred for applications of SAPT(DFT), especially the PBE0 hybrid functional (with an asymptotic correction term to achieve correct long-range behavior of the potential). 10,49 However, the use of hybrid functionals complicates the dispersion and exchangedispersion terms, requiring either computational steps that scale as $O(N^5)$ [compared to $O(N^4)$ without the use of a hybrid kernel for dispersion] or else the construction of a local representation of the Hartree-Fock potential (LHF) that can then be used with a simpler ALDA kernel in the treatment of dispersion. Although the latter choice formally scales as only $O(N^4)$, in practice, the LHF equations can be hard to converge and thus may require substantial time. Here, we have implemented an $O(N^5)$ algorithm allowing the hybrid kernel to be used for dispersion based on the algorithm of Bukowski et al.27

^b Including integral transformation, form X/form Y (the $O(N^5)$ part), and QR factorization. In Molpro, the integral transformation is integrated with other terms, and the other steps are not relevant for LHF.

We have improved this algorithm by using a 2-index representation of the exchange–correlation kernel as proposed by Pitoňák and Hesselmann³⁰ and by improving the numerical stability replacing the "projector" in Bukowski's work (Ref. 27) with a pseudoinverse operation based on QR factorization. We have also optimized the tensor contraction procedures to minimize disk I/O, which affects the efficiency of the algorithm heavily as the system size increases.

Our algorithm scales as $O(N^5)$ formally in the dispersion and exchange-dispersion term, but in practice, the iterative $O(N^4)$ induction term usually contributes a non-negligible or even dominating portion to the total computational cost, especially for small or medium-sized systems with less than 2000 basis functions. Timings of each step in the algorithm justify our choice of the SAPT(DFT) algorithm based on hybrid xc-kernel over the LHF approach because in most systems that are small enough to be computed with SAPT(DFT), the prefactor is shown to have more influence on the total computational cost than the formal scaling.

Using the new code, we examined the accuracy of SAPT(DFT) using the hybrid kernel for dispersion comparing to the LHF-based treatment and also with the results obtained using PBE0AC with neither LHF orbitals nor a hybrid kernel for dispersion. The latter approach is not as accurate as the former two, but LHF-based SAPT(DFT) and hybrid-kernel-based SAPT(DFT) give very similar results once we reformulate the scaling factor used to estimate the coupled exchange-dispersion energy from the uncoupled exchangedispersion energy. The appropriate scaling factor is shown here to be heavily dependent of whether the DFT algorithm used to generate the molecular orbitals adopts the LHF approximation. Based on the results for diverse non-covalent interactions in the S66 test set, the SAPT(DFT) results are generally more accurate than their SAPT0 counterparts, with the exception of the exchange component. The mean absolute error of SAPT(DFT) is comparable to that of SAPT2+, which scales as $O(N^7)$ as opposed to $O(N^5)$ for hybrid-kernel SAPT(DFT), for the total interaction energy and all components except for exchange, although the error distributions are wider for SAPT(DFT).

SUPPLEMENTARY MATERIAL

See the supplementary material for complete tables of all energetic quantities reported in this work (SAPT components and total interaction energies). In addition, a table comparing SAPT2+3(CCD) δ MP2/aug-cc-pVTZ to SAPT(CCSD)/aug-cc-pVTZ for S2 and tables comparing our results for S2 to SAPT0/aug-cc-pVTZ and our S66 results to SAPT0/aug-cc-pVTZ and SAPT2+/aug-cc-pVTZ are provided.

ACKNOWLEDGMENTS

The authors gratefully acknowledge financial support from the U.S. National Science Foundation through Grant No. CHE-1955940. We thank Zach Glick for assistance in analyzing the PSI4 timing results and Professor Konrad Patkowski (Auburn University) for helpful comments.

AUTHOR DECLARATIONS

Conflict of Interest

The authors have no conflicts to disclose.

Author Contributions

Yi Xie: Data curation (lead); Formal analysis (equal); Investigation (lead); Methodology (lead); Software (equal); Validation (lead); Writing-original-draft (lead). Daniel G. A. Smith: Investigation (supporting); Methodology (supporting); Software (equal). C. David Sherrill: Conceptualization (lead); Formal analysis (equal); Funding acquisition (lead); Project administration (lead); Resources (lead); Supervision (lead); Writing-original-draft (supporting); Writing-review-editing (lead).

DATA AVAILABILITY

The data that support the findings of this study are available within the article and its supplementary material.

REFERENCES

- ¹B. Jeziorski, R. Moszynski, and K. Szalewicz, Chem. Rev. **94**, 1887 (1994).
- ² K. Szalewicz, Wiley Interdiscip. Rev.: Comput. Mol. Sci. **2**, 254 (2012).
- ³E. G. Hohenstein and C. D. Sherrill, Wiley Interdiscip. Rev.: Comput. Mol. Sci. 2, 304 (2012).
- ⁴C. D. Sherrill, Acc. Chem. Res. 46, 1020 (2013).
- ⁵H. L. Williams and C. F. Chabalowski, J. Phys. Chem. A 105, 646 (2001).
- ⁶J. P. Perdew and M. Levy, Phys. Rev. Lett. **51**, 1884 (1983).
- ⁷G. Jansen and A. Heßelmann, J. Phys. Chem. A **105**, 11156 (2001).
- ⁸A. Heßelmann and G. Jansen, Chem. Phys. Lett. **362**, 319 (2002).
- ⁹K. Patkowski, K. Szalewicz, and B. Jeziorski, Theor. Chem. Acc. 127, 211 (2010)
- ¹⁰ A. Heßelmann and G. Jansen, Chem. Phys. Lett. 357, 464 (2002).
- ¹¹J. P. Perdew, K. Burke, and M. Ernzerhof, Phys. Rev. Lett. 77, 3865 (1996).
- ¹²C. Adamo and V. Barone, J. Chem. Phys. **110**, 6158 (1999).
- ¹³R. van Leeuwen and E. J. Baerends, *Phys. Rev. A* **49**, 2421 (1994).
- ¹⁴M. Grüning, O. V. Gritsenko, S. J. A. van Gisbergen, and E. J. Baerends, J. Chem. Phys. 114, 652 (2001).
- ¹⁵ A. J. Misquitta and K. Szalewicz, Chem. Phys. Lett. **357**, 301 (2002).
- ¹⁶E. Fermi and E. Amaldi, Mem. R. Acad. Italia 6, 117 (1934).
- ¹⁷D. J. Tozer and N. C. Handy, J. Chem. Phys. **109**, 10180 (1998).
- ¹⁸G. Jansen, Wiley Interdiscip. Rev.: Comput. Mol. Sci. 4, 127 (2014).
- ¹⁹ A. J. Misquitta and K. Szalewicz, J. Chem. Phys. **122**, 214109 (2005).
- ²⁰ A. Heßelmann and G. Jansen, Chem. Phys. Lett. **367**, 778 (2003).
- ²¹ A. J. Misquitta, R. Podeszwa, B. Jeziorski, and K. Szalewicz, J. Chem. Phys. 123, 214103 (2005).
- ²²E. J. Baerends, D. E. Ellis, and P. Ros, Chem. Phys. 2, 41 (1973).
- ²³ J. L. Whitten, J. Chem. Phys. **58**, 4496 (1973).
- ²⁴S. J. A. van Gisbergen *et al.*, Phys. Rev. A **57**, 2556 (1998).
- ²⁵ A. Heßelmann, G. Jansen, and M. Schütz, J. Chem. Phys. **122**, 014103 (2005).
- ²⁶ A. J. Misquitta, B. Jeziorski, and K. Szalewicz, Phys. Rev. Lett. 91, 033201 (2003).
- ²⁷R. Bukowski, R. Podeszwa, and K. Szalewicz, Chem. Phys. Lett. **414**, 111 (2005).
- ²⁸F. Della Sala and A. Görling, J. Chem. Phys. **115**, 5718 (2001).

- ²⁹R. Bukowski *et al.*, SAPT2020: An *ab initio* program for many-body symmetry-adapted perturbation theory calculations of intermolecular interaction energies, University of Delaware and University of Warsaw, 2020.
- ³⁰M. Pitoňák and A. Heßelmann, J. Chem. Theory Comput. **6**, 168 (2010).
- ³¹ Y. C. Zheng and J. Almlöf, Chem. Phys. Lett. **214**, 397 (1993).
- ³²Y. C. Zheng and J. E. Almlöf, J. Mol. Struct.: THEOCHEM **388**, 277 (1996).
- ³³K. R. Glaesemann and M. S. Gordon, J. Chem. Phys. **108**, 9959 (1998).
- ³⁴ A. Heßelmann and T. Korona, J. Chem. Phys. **141**, 094107 (2014).
- 35 L. Gráfová, M. Pitoňák, J. Řezáč, and P. Hobza, J. Chem. Theory Comput. 6, 2365 (2010).
- ³⁶J. Řezáč, K. E. Riley, and P. Hobza, J. Chem. Theory Comput. 7, 2427 (2011).
- ³⁷J. Řezáč, K. E. Riley, and P. Hobza, J. Chem. Theory Comput. **10**, 1359 (2014).
- ³⁸ J. Řezáč, K. E. Riley, and P. Hobza, J. Chem. Theory Comput. 7, 3466 (2011).
- ³⁹D. G. A. Smith L. A. Burns, A. C. Simmonett, R. M. Parrish, M. C. Schieber, R. Galvelis, P. Kraus, H. Kruse, R. Di Remigio, A. Alenaizan, A. M. James, S. Lehtola, J. P. Misiewicz, M. Scheurer, R. A. Shaw, J. B. Schriber, Y. Xie, Z. L. Glick, D. A. Sirianni, J. Senan O'Brien, J. M. Waldrop, A. Kumar, E. G. Hohenstein, B. P. Pritchard, B. R. Brooks, H. F. Schaefer III, A. Yu. Sokolov, K. Patkowski, A. E. DePrince III, U. Bozkaya, R. A. King, F. A. Evangelista, J. M. Turney, T. D. Crawford, and C. D. Sherrill, J. Chem. Phys. 152, 184108 (2020).
- ⁴⁰ R. Podeszwa, R. Bukowski, and K. Szalewicz, J. Chem. Theory Comput. 2, 400 (2006).
- ⁴¹ K. Raghavachari, G. W. Trucks, J. A. Pople, and M. Head-Gordon, Chem. Phys. Lett. 157, 479 (1989).
- ⁴² A. Heßelmann, "Die Berechnung von intermolekularen wechselwirkungsbeiträgen mit dichtefunktional- und Brueckner-coupled-cluster-methoden," Ph.D. thesis, University Duisburg-Essen, Essen, 2003.
- ⁴³J. P. Perdew, R. G. Parr, M. Levy, and J. L. Balduz, Jr., Phys. Rev. Lett. **49**, 1691 (1982).

- 44 M. Jaszunski and R. McWeeny, Mol. Phys. 55, 1275 (1985).
- ⁴⁵P. J. Knowles and W. J. Meath, Mol. Phys. **59**, 965 (1986).
- ⁴⁶J. Garcia and K. Szalewicz, J. Chem. Phys. A **124**, 1196 (2020).
- ⁴⁷T. H. Dunning, Jr., J. Chem. Phys. **90**, 1007 (1989).
- ⁴⁸ R. A. Kendall, T. H. Dunning, Jr., and R. J. Harrison, J. Chem. Phys. **96**, 6796 (1992).
- 49 T. Korona, Mol. Phys. 111, 3705 (2013).
- ⁵⁰ T. M. Parker, L. A. Burns, R. M. Parrish, A. G. Ryno, and C. D. Sherrill, J. Chem. Phys. **140**, 094106 (2014).
- ⁵¹ H. L. Williams, K. Szalewicz, R. Moszynski, and B. Jeziorski, J. Chem. Phys. 103, 4586 (1995).
- ⁵² MOLPRO, version 2019.2, a package of *ab initio* programs, H.-J. Werner, P. J. Knowles, G. Knizia, F. R. Manby, M. Schütz, P. Celani, W. Györffy, D. Kats, T. Korona, R. Lindh, A. Mitrushenkov, G. Rauhut, K. R. Shamasundar, T. B. Adler, R. D. Amos, S. J. Bennie, A. Bernhardsson, A. Berning, D. L. Cooper, M. J. O. Deegan, A. J. Dobbyn, F. Eckert, E. Goll, C. Hampel, A. Heßelmann, G. Hetzer, T. Hrenar, G. Jansen, C. Köppl, S. J. R. Lee, Y. Liu, A. W. Lloyd, Q. Ma, R. A. Mata, A. J. May, S. J. McNicholas, W. Meyer, T. F. Miller III, M. E. Mura, A. Nicklass, D. P. O'Neill, P. Palmieri, D. Peng, T. Petrenko, K. Pflüger, R. Pitzer, M. Reiher, T. Shiozaki, H. Stoll, A. J. Stone, R. Tarroni, T. Thorsteinsson, M. Wang, and M. Welborn, see https://www.molpro.net.
- ⁵³F. Weigend and R. Ahlrichs, Phys. Chem. Chem. Phys. 7, 3297 (2005).
- ⁵⁴P. Jurečka, J. Šponer, J. Černý, and P. Hobza, Phys. Chem. Chem. Phys. 8, 1985 (2006).
- 55 C. Mück-Lichtenfeld, S. Grimme, L. Kobryn, and A. Sygula, Phys. Chem. Chem. Phys. 12, 7091 (2010).
- ⁵⁶R. Podeszwa, W. Cencek, and K. Szalewicz, J. Chem. Theory Comput. 8, 1963 (2012).